Chemical Science

ROYAL SOCIETY OF CHEMISTRY

EDGE ARTICLE

View Article Online
View Journal | View Issue

Cite this: *Chem. Sci.*, 2026, **17**, 1694

All publication charges for this article have been paid for by the Royal Society of Chemistry

High-performance narrowband blue electroluminescence with EQE approaching 20% based on hybridized local and charge-transfer multi-resonant molecules

Huihui Li,†[a] Jiayi Qin,†[b] Taotao Ma,[a] Jiajie Zeng,[b] Ziwei Chen,[b] Yan Fu,[b] Hua Lu,*[a] Zujin Zhao*[b] and Xin Jiang Feng*[a]

Received 16th August 2025
Accepted 18th November 2025

DOI: 10.1039/d5sc06259d

rsc.li/chemical-science

Designing multi-resonant (MR) materials that integrate narrowband emission and efficient exciton utilization remains challenging, especially for indolocarbazole (ICz) cores. To address this, two novel ICz-derived MR emitters, 4CzmICz and 4CzpICz, were developed by strategically extending π-conjugation *via* peripheral carbazole units. This modulates charge-transfer (CT) states while retaining MR character, endowing both molecules with hybridized local and charge transfer (HLCT) properties. The *meta*-isomer 4CzmICz exhibits exceptional deep-blue emission (430 nm, FWHM = 14 nm in hexane). The *para*-isomer 4CzpICz achieves record HLCT-OLED performance: a narrowband device (FWHM = 29 nm) with 19.5% external quantum efficiency (EQE). In an exciplex-sensitized configuration, EQE reaches 25.0% without emission broadening. This work pioneers MR-HLCT integration and establishes a roadmap for next-generation OLED materials.

1 Introduction

Driven by the demand for next-generation ultrahigh-definition (UHD) displays, organic light-emitting diodes (OLEDs) with high electroluminescence (EL) efficiency and superior color fidelity have garnered significant attention.[1–9] While organic emitters offer notable advantages such as facile synthesis, mechanical flexibility, large-area fabrication compatibility, and color tunability, commercially available systems typically exhibit broad emission spectra with full width at half maximum (FWHM) of >40 nm.[10–12] Particularly, to achieve 100% exciton utilization, researchers have extensively developed emitters with long-range charge transfer (CT) states, including phosphorescent materials,[13–17] thermally activated delayed fluorescence (TADF) emitters,[18–24] and hybridized local and charge-transfer (HLCT) systems.[25–28] However, these materials often suffer from substantial vibrational relaxation at excited states (S_1 or T_1), leading to broader emission spectra. To address this issue, a novel molecular design strategy has emerged: emitters featuring non-bonding orbitals with spatially separated HOMO and LUMO distributions on single atoms. This approach, achieved by embedding heteroatoms with opposing resonance effects into polycyclic aromatic hydrocarbon frameworks, has enabled narrowband emission.[29,30] Until now, multiple resonance (MR) emitters, particularly those incorporating *ortho*-positioned boron (B) and nitrogen (N) atoms, have shown remarkable progress.[31–36] Despite their potential, MR emitters face dual challenges: (1) complex synthetic routes requiring alkyllithium-mediated lithiation for boron incorporation, often yielding low efficiency and (2) a lack of blue emitters with both efficiency and fast spin-flipping.[4,37–42]

An alternative breakthrough was pioneered by Lee *et al.*, who demonstrated that fusing indolo[3,2,1-*jk*]carbazole (ICz) units, a nitrogen-centered tripodal structure surrounded by aromatic rings, could induce an MR effect through the contrast electronegativity between carbon and nitrogen.[38,39,43–48] This design spatially separates HOMO and LUMO distributions on distinct carbon atoms, yielding an unprecedentedly narrow EL spectrum (FWHM = 14 nm, the smallest reported to date). While these systems show compelling advantages, their current EQEs remain limited to 3.3% and 15.1%, underscoring the necessity for further exploration into molecular engineering to enhance performance.

Herein, we developed two novel MR emitters (4CzmICz and 4CzpICz) by functionalizing the ICz core with four carbazolyl groups exhibiting exceptional thermal stability (T_d = 530–540 °

[a]*Key Laboratory of Organosilicon Chemistry and Material Technology, Ministry of Education, Zhejiang Key Laboratory of Organosilicon Material Technology, College of Material, Chemistry and Chemical Engineering, Hangzhou Normal University, Hangzhou, 311121, Zhejiang, China. E-mail: hualu@hznu.edu.cn; xjfeng@hznu.edu.cn*

[b]*State Key Laboratory of Luminescent Materials and Devices, Guangdong Provincial Key Laboratory of Luminescence from Molecular Aggregates, South China University of Technology, Guangzhou, 510640, Guangdong, China. E-mail: mszjzhao@scut.edu.cn*

† H. L. and J. Q. contributed equally to this work.

C). The 4CzmICz-based OLED achieved deep-blue emission at 424 nm with CIE (0.167, 0.045) and 27 nm FWHM, while 4CzpICz delivered a record high 19.5% EQE in pure-blue device (29 nm FWHM) – the first HLCT system approaching 20% EQE. This work advances HLCT design principles for high-performance blue emitters.

2 Results and discussion

2.1 Molecular design strategy

For ICz units, locally excited (LE) excitons will rapidly relax to the ground state (S_0) by radiating photons, it does not facilitate reverse intersystem crossing (RISC). Consequently, the EQE of the ICz core remains limited. To address this, we engineered charge-transfer (CT) character into the excited states by strategically introducing electron-donating carbazole units to the electron-deficient MR core. This molecular design creates a hybrid excited state that combines the narrow emission characteristics of MR materials through their alternating HOMO–LUMO distributions (Fig. 1) and enhances RISC efficiency *via* the D–A interaction-induced CT component. The carbazole substituents serve dual functions. Electronically, they mediate the HLCT character by hybridizing MR and CT states and, they sterically suppress detrimental intermolecular interactions. As evidenced by frontier molecular orbitals (FMOs) analysis, this design successfully achieves spatial separation of LUMO (localized on the MR core with characteristic alternating distribution) and HOMO (delocalized across the entire molecule), while maintaining minimal geometry changes between ground and excited states (Fig. S1 and S2) – a crucial factor for preserving narrowband emission.

The synthetic routes for the molecules are outlined in Scheme S1. Starting from 3,6-di-tertbutylcabazole, compound **4** was synthesized by amino-protection, Buckwald–Hartwig reaction for amination and debenzylation. The subsequent nucleophilic aromatic substitution reaction of compound **4** with 1,4-dibromo-2,5-difluorobenzene and 1,5-dibromo-2,4-difluorobenzene gave the key intermediates compound **5** and **6**, respectively. Finally, the target molecules, 4CzmICz and 4CzpICz, were obtained efficiently *via* the ring–closing reaction with palladium catalysis. Both target molecules were characterized by ^{1}H NMR, ^{13}C NMR spectroscopy, and high-resolution mass spectrometry.

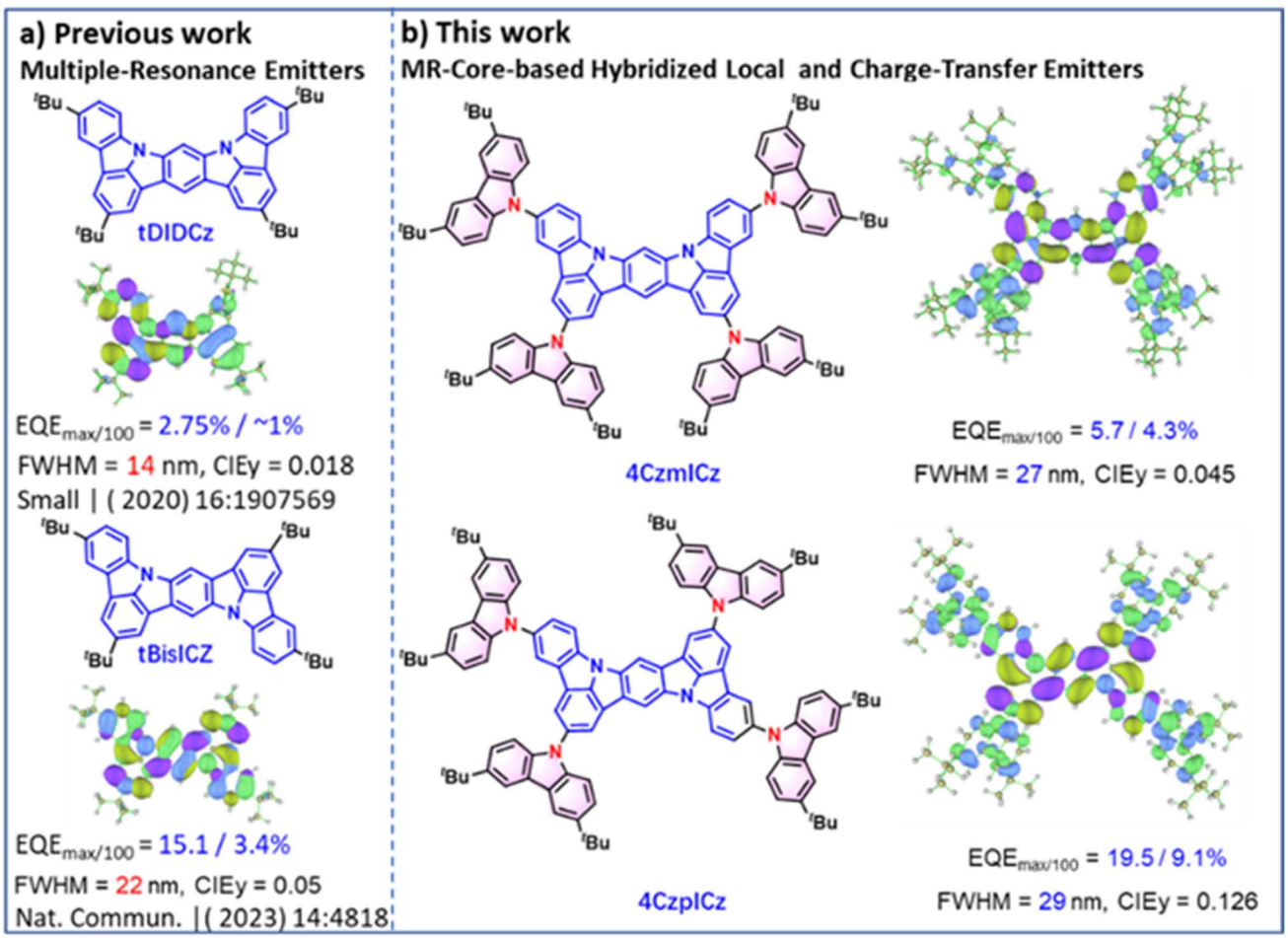

Fig. 1 Design strategy. Molecular structures and HOMO(green/blue)–LUMO(purple/yellowish green) distributions calculated by M062X/6-31G(d) for (a) the previous work and (b) the current work.

2.2 Quantum chemical calculation

The FMOs and the optimized structures in the ground and excited states together with their torsion angles are calculated by density functional theory (DFT) and displayed in Fig. 1 and S3. The LUMOs of both molecules are located on the ICz central cores and exhibit apparently alternate distribution on the carbon atoms *ortho*-position to the nitrogen atoms. The HOMOs are delocalized in the whole molecules, exhibiting the alternate distribution characteristics. Such HOMO–LUMO distributions show typical multi-resonant HLCT character. However, 4CzpICz shows more evenly distributed HOMO and has a stronger distribution on the central ICz core compared to 4CzmICz, due to the stronger conjugation deriving from the *para*-positoned nitrogens. This results in the different overlaps of HOMO–LUMO and 4CzpICz shows more LE component. The rigid carbazolyl peripheral units show only small rotations around the C–N bond. The rigid structures and small change between S_0 and S_1 can reduce the vibrations and the nonradiative transitions, which helps to achieve high efficiency and good color purity with narrow-spectrum emission (Fig. S1 and S2). The calculated root means square deviation (RMSD) values are only 0.246 and 0.253 Å between S_0 and S_1 during the excitation process for 4CzmICz and 4CzpICz, respectively, indicating the suppressed vibrational relaxation (Fig. 2a and b).[49–51] Small total reorganization energies were calculated as ~0.22 and 0.23 eV for 4CzmICz and 4CzpICz, respectively, indicating the weak electron–phonon coupling—consistent with its narrowband emission property (Fig. 2c and d).

To study the excited transitions in these molecules, time-dependant (TD) DFT calculations were made by M062X functional with 6-31G(d) basis sets (Tables S1 and S2). Apart from the strong transition from HOMO to LUMO with large oscillator strength, HOMO−1 and LUMO+1 participate in the lowest transitions significantly, infering their strong fluorescence of both molecules. To explore deep into the excited-state characteristics, natural transition orbital (NTO) calculations was performed (Fig. S4 and S5). For both molecules, the NTO "holes" and "particles" of the singlet states and triplet states are partially overlaped or seperated, showing the HLCT character of the elecronic structures. The LE components are beneficial to improve the fluorescence quantum efficiency (Φ_F) and reduce red-shift in fluorescence. While the CT states help to reverse intersystem crossing from triplet states to singlet states. The NTO calculations show that the appending donor groups on the ICz cores can fine tune the LE and CT states of the molecules.

For further understanding the exciton utility, the energy levels of the singlet and triplet states are studied (Fig. 2e and f). Usually, a small energy splitting of less than 0.1 eV between S_1 and T_1 (ΔE_{S1-T1}) is need to conduct an efficient themally activated delayed fluorescence (TADF) process in electroluminescence device. The ΔE_{S1-T1} are as wide as 0.886 and 0.765 eV for 4CzmICz and 4CzpICz, respectively, which dosen't favour a TADF process in RISC. In addition, large energy gaps are also

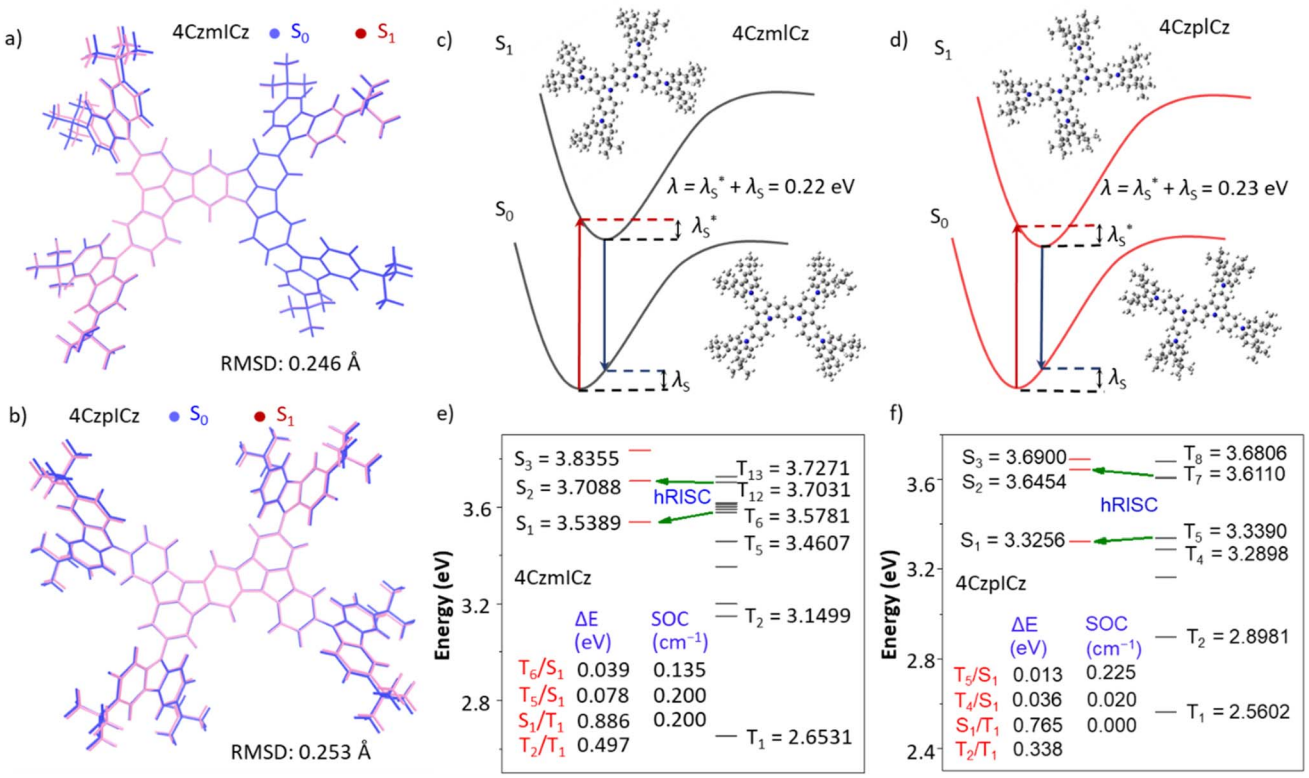

Fig. 2 (a and b) RMSD between the S_0 and S_1 geometries. (c and d) reorganization energy. (e and f) Singlet and triplet excited states calculated by TD-M062X/6-31G(d) for 4CzmICz and 4CzpICz.

found between the highlying triplet states and T_1, and thus such transitons are confined to show reduced nonradiative decay. Nevertheless, very small splitting energies are found between the high-lying triplet transitions and the singlet transitions. For example, the splitting energies are as small as 0.078 and 0.013 eV of T_5/S_1 for 4CzmICz and 4CzpICz, respectively. In contrast, significant spin–orbit coupling (SOC) between T_5 and S_1 are found of 0.200 cm^{-1} (4CzmICz) and 0.225 cm^{-1} (4CzpICz). These results indicate the effective coupling between the high lying triplet excited states (T_n, $n \geq 2$) and singlet states (S_m, $m \geq 1$), which makes the RISC from triplet state to singlet state possible.

2.3 Thermal, morphological, photophysical and electrochemical stability

The thermal properties of the materials were determined by differential scanning calorimetry (DSC) and thermogravimetric analysis (TGA) measurements. The materials exhibit excellent thermal stability with high decomposition temperatures of 530 and 540 °C for 4CzmICz and 4CzpICz, respectively. There are no glass transition temperatures detected for both materials from 30 to 300 °C, indicating the morphological stability of the materials in a wide range of measurement. These results indicate that both materials are favorable for solid-state applications and suitable for a sublimate process in OLED fabrication (Fig. S6).

The photophysical properties of 4CzmICz and 4CzpICz were measured in solution and thin films (Fig. 3a, S7, Tables 1, and S3). In toluene solution, the maximum absorption peaks around 345 nm for 4CzmICz and 346 nm for 4CzpICz can be ascribe to the π–π* transitions in the carbazole units and the ICz cores, while the absorptions peaking at 411 and 447 nm belong to the CT transitions in the molecules. The absorption spectra show minimal solvent dependence, suggesting small ground-state dipole moments in both emitters. 4CzmICz and 4CzpICz exhibit medium to high fluorescence quantum efficiencies in the deep-blue to pure-blue region with narrowband emissions (FWHM : 4CzmICz = 14–40 nm, 4CzpICz = 20–45 nm). Owing to the medium φ_{PL}s of the emitters under 320 nm excitation, the calculated radiative constants are as large as 5.7 × 10^7 and 4.1 × 10^7 s^{-1}. The emission spectra of 4CzmICz displays a 17 nm red-shift from hexane to acetonitrile, while 4CzpICz shows only 8 nm shift, indicating weaker CT character. The *para*-substituted 4CzpICz exhibits particularly suppressed CT effects due to its symmetric structure. Additionally, the small Stokes shifts observed consistent with minor geometric relaxation in the emissive state, further support the dominance of LE states over CT contributions.[52]

The Lippert–Mataga plots (Fig. 3c and d) reveal the electronic properties of the emitters by correlating Stokes shifts with solvent polarizability. Both molecules exhibit two distinct linear regions, indicating hybridized local and charge-transfer (HLCT) character—LE-like states dominate in nonpolar solvents (small μ_e), while CT-like states prevail in polar solvents (large μ_e).[53] In 1 wt% doped films, both emitters maintain intense, narrowband emission (FWHM = 33 nm). Compared to the high doping films, the 1 wt% doped film has a smaller effect of concentration quenching. While compared to the solutions, the emitter has a confined environment with less vibration and rotation, which reduces the nonradiative emission and helps to achieve a high quantum yield. Notably, 4CzpICz achieves near-unity photoluminescence quantum yield (98.6%) at this concentration, demonstrating exceptional potential as a terminal emitter in hyperfluorescence devices.

To investigate the triplet utility, the absolute fluorescence quantum yields and fluorescence lifetimes in toluene solutions were measured. Under nitrogen, the fluorescence lifetimes enhanced slightly and kept at nanosecond levels for both molecules (Fig. 3e, S8 and Table S4). As listed in Table S4, obvious increases in fluorescence were observed at −78 °C, and the variations of quantum yields are comparatively small at other temperatures. At a low temperature of −78 °C, the rotation and vibration motions in the molecules are significantly reduced, thus leading to the reduction of nonradiative decay and the in the increase of fluorescence. For the same reason, the emission spectra are narrowed to 12 and 15 nm for 4CzmICz and 4CzpICz, respectively. However, significant enhancements of quantum yields were detected in solutions under nitrogen as compared to those under air, which clearly indicates the triplet participation during the fluorescent process. To get further information about the mechanism of triplet utility, transient PL spectra depending on temperature were measured in toluene solution and in thin films with 1 wt% emitters in mCP (Fig. 3f and S9). On one hand, single exponential decay curves and nanosecond-scale lifetime of the solutions and doped films were detected, indicating no significantly long-time delayed fluorescence in the emission (Table 1). On the other hand, no positive response of fluorescence to increase of temperature was observed at ns-scales and μs-scales in the transient PL, which indicates no TADF in the emission process.

The electrochemical property of 4CzmICz and 4CzpICz was investigated by cyclic voltammetry (CV) performed in 0.1 M Bu_4NPF_6 dichloromethane or dimethylformamide (Table 1 and Fig. S10). The onset potentials are 0.79/−2.47 and 0.70/−2.10 eV for 4CzmICz and 4CzpICz, respectively. The onset potentials of Fc/Fc^+ were measured as 0.10 V for oxidation and 0.01 V for reduction. By $E_{HOMO/LUMO} = -(4.8\ eV + E_{onset} - E_{onset/Fc/Fc^+})$, the HOMOs/LUMOs are calculated to be −5.49/−2.32 (4CzmICz) and −5.40/−2.69 eV (4CzpICz). The HOMO/LUMO energy levels of these dyes change obviously with the different conjugation and the *para* molecules has a lower energy gap for the comparatively strong conjugation. According to $E_g = E_{HOMO} - E_{LUMO}$, the energy gaps ($E_g$) are calculated to be 3.17 eV (4CzmICz) and 2.71 eV (4CzpICz), which show the near potential with optical E_g estimated from the absorbing spectra in toluene solutions to be 2.90 and 2.67 eV for 4CzmICz and 4CzpICz, respectively. The large E_gs indicate that the dyes are suitable for blue emission.

2.4 Device fabrication and evaluation

Bottom-emission OLEDs were fabricated using the dyes as emitters doping into mCP (host) or TSOP1/mCP (cohost) with

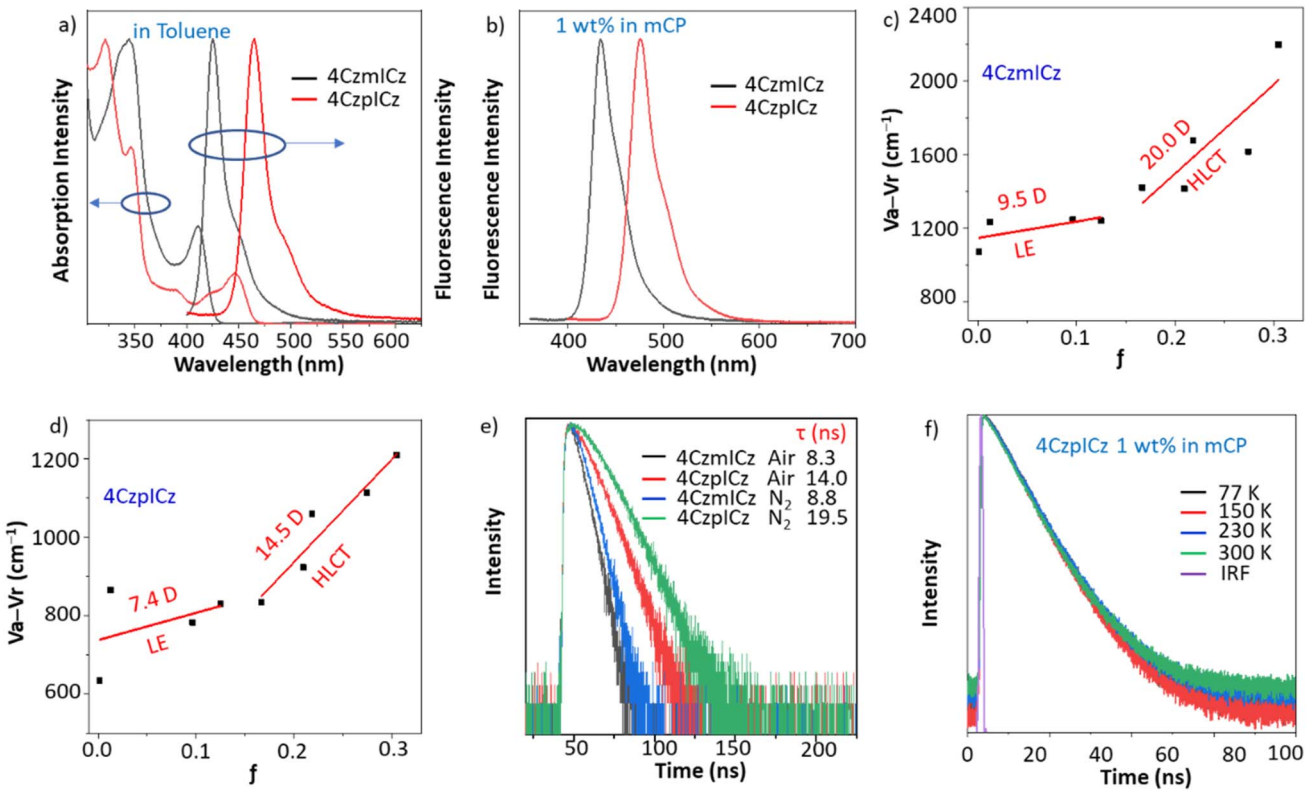

Fig. 3 (a) Absorption and emission spectra in toluene solutions (10^{-5} M for absorption and 10^{-6} M for emission). (b) Emission in doped films. (c and d) Lippert–Mataga plots (Stokes shifts versa solvent polarizabilties) and the linear fittings for 4CzmICz and 4CzpICz. (e) Transient PL spectra of the emitters under air/nitrogen at room temperature in toluene solutions. (f) Temperature dependant transient PL spectra in doped film for 4CzpICz (1 wt% in mCP) under nitrogen.

the structures of ITO/HATCN (5 nm)/TAPC (50 nm)/TCTA (5 nm)/mCP (5 nm)/EML (20 nm)/TSPO1 (5 nm)/TmPyPB (30 nm)/LiF (1 nm)/Al, EML (emitting layer) = 1 wt% 4CzmICz: mCP (D1), 1 wt% 4CzmICz: 50 wt% TSPO1: mCP (S1), 1 wt% 4CzpICz: mCP (D2), 1 wt% 4CzpICz: 50 wt% TSPO1: mCP (S2). In which, indium tin oxide (ITO) is transparent anode; dipyrazino[2,3-*f*:2′,3′-*h*]quinoxaline-2,3,6,7,10,11-hexacarbonitrile (HATCN) is applied as a hole injection layer; 4,4′-cyclohexylidenebis[*N*,*N*-bis(4-methylphenyl)aniline] (TAPC) is a hole-transporting layer; tris[4-(carbazol-9-yl)phenyl]amine (TCTA) and 1,3-di-9-carbazolylbenzene (mCP) functions as an electron-blocking layer; EML is the emitting layer (mCP served as host, TSPO1 served as cohost to construct exciplex with mCP in sensitized devices); diphenyl[4-(triphenylsilyl)phenyl]phosphine oxide (TSPO1) is used as an exciton-blocking layer; 1,3,5-tri(*m*-pyrid-3-yl-phenyl)benzene (TmPyPB) is utilized as an electron-transporting layer, and LiF/Al works as cathode (Fig. 4a).

As shown in Table 2 and Fig. 4b–d, the device D1 incorporating 1 wt% 4CzmICz emitter, demonstrates exceptional deep-blue emission at 424 nm with outstanding color purity (FWHM = 27 nm, CIEy = 0.045), meeting the stringent BT.2020 blue standard. This device achieves peak performance metrics of 1051 cd m^{-2} luminance, 2.0 cd A^{-1} current efficiency, 1.7 lm W^{-1} power efficiency, and 5.7% EQE. Remarkably, the D2 device with 1 wt% 4CzpICz emitter delivers pure-blue emission at 468 nm while maintaining narrowband characteristics (FWHM = 29 nm), achieving record-breaking performance: 3866 cd m^{-2} luminance, 19.4 cd A^{-1} current efficiency, 16.9 lm W^{-1} power efficiency, and 19.5% EQE. This represents the highest reported efficiency for HLCT-based OLEDs to date, preserving the MR

Table 1 Photophysical properties in toluene solutions and electrochemical properties of 4CzmICz and 4CzpICz

Compd	λ_{abs} [a] (nm)	λ_{em} [a] (nm)	$\Delta\nu_{em-abs}$ [b] (cm^{-1})	FWHM [c] (nm)	Φ_F [d] (%)	τ_F [e] (ns)	k_r/k_{nr} [f] (10^7 s^{-1})	E_{onset} [g] (V)	HOMO/LUMO/E_g [h] (eV)
4CzmICz	345/411	433	1236	20	0.37/0.50	8.3/8.8	5.7/5.7	0.79/−2.47	−5.49/−2.32/3.17
4CzpICz	346/447	465	866	24	0.40/0.58	14.0/19.5	4.1/3.0	0.70/−2.10	−5.40/−2.69/2.71

[a] Main absorption and emission peaks. [b] Stokes' shifts. [c] Full width at half maximum. [d] Fluorescence quantum yields under air/nitrogen. [e] The fluorescence lifetime under air/nitrogen excited at 365 nm. [f] Radiative and nonradiative constant. [g] Oxidation (dichloromethane as solvent)/reduction (*N*,*N*-dimethylformamide as solvent) potentials from cyclic voltammetry, $Ag/AgNO_3$ was used as a reference. [h] HOMO, LUMO, and E_g (energy gap) obtained from CV measurement.

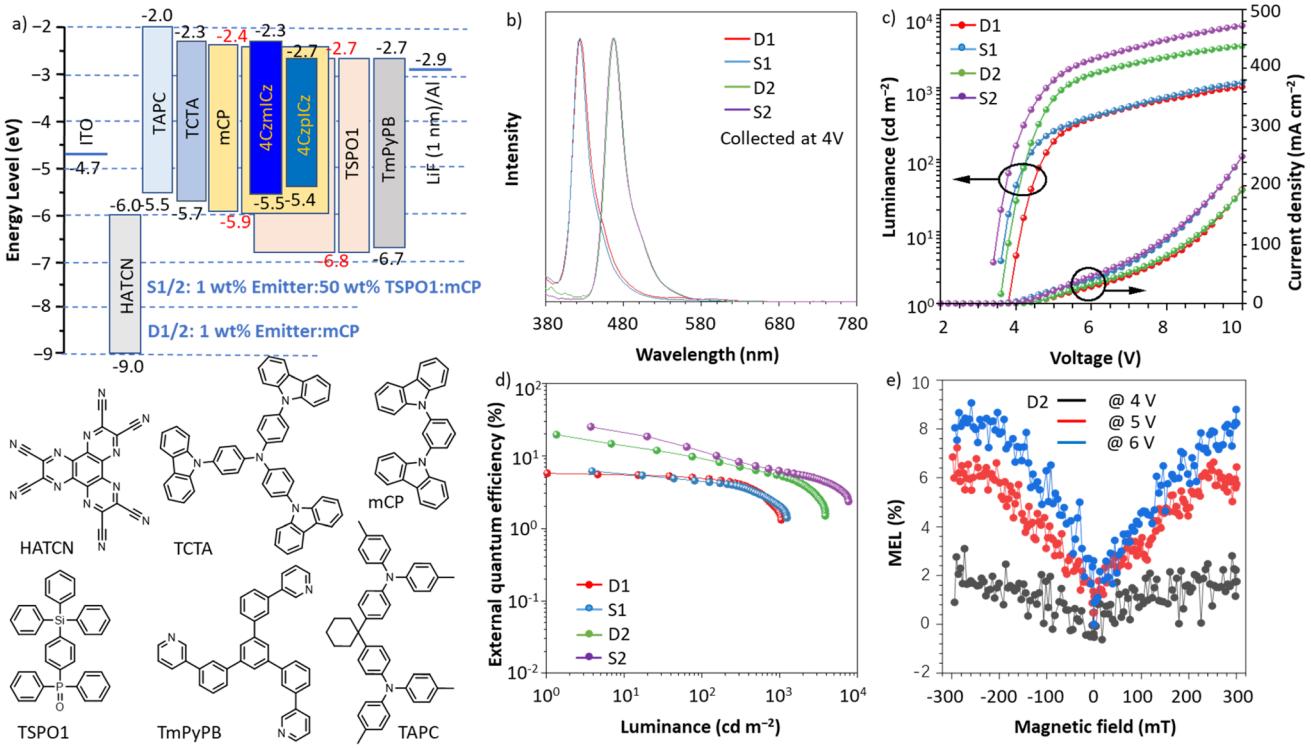

Fig. 4 (a) Device structures, molecular structures and energy levels. (b) EL spectra of OLEDs. (c) Luminance and current density *vs.* voltage. (d) EQE *vs.* luminance. (e) MEL curves of the 4CzmICz- and 4CzpICz-based OLEDs at different voltages (device configuration: DI ITO/HATCN (5 nm)/TAPC (50 nm)/TcTa (5 nm)/mCP (5 nm)/1 wt% 4CzmICz: mCP (20 nm)/TSPO1 (5 nm)/TmPyPB (30 nm)/LiF (1 nm)/Al; DII ITO/HATCN (5 nm)/TAPC (50 nm)/TcTa (5 nm)/mCP (5 nm)/1 wt% 4CzpICz: mCP (20 nm)/TSPO1 (5 nm)/TmPyPB (30 nm)/LiF (1 nm)/Al).

character (Table S5). Considering the high EQEs of both devices, the exciton utility efficiency (EUE) are calculated by eqn (1), in which γ is a balance factor of carriers (100%), η_{PL} is the fluorescent efficiencies (0.649 for 4CzmICz and 0.986 for 4CzpICz) of the films with 1 wt% doping concentration, and η_{out} stands for the light out-coupling factor ($\approx$0.25 for ITO substrate), we calculated EUE values of 35% (D1) and 79% (D2). These results confirm efficient triplet exciton harvesting in both devices. As discussed in theoretical calculations, the energy difference between T_1 and S_1 are large both molecules, which hinders the reverse conversion from T_1 state to S_1 state. Combined with their nanosecond-scale fluorescence lifetimes, this rules out TADF as the primary exciton harvesting mechanism. Furthermore, the absence of nonlinear luminance-current density dependence at low currents (Fig. S11) excludes triplet–triplet annihilation (TTA) as a dominant process. At the meanwhile, small energy differences and strong SOC are found in the excited states, such as T_{5-6}/S_1 for 4CzmICz and T_5/S_1 for 4CzpICz, facilitating the high-lying RISC process. Therefore, the triplet exciton utility can be ascribed to an HLCT process.

$$\eta_{ext} = \gamma \times \eta_{PL} \times \eta_r \times \eta_{out} \quad (1)$$

Transient EL test (Fig. S12) detected microsecond-scale lifetimes of 14.8 μs for 4CzmICz-based OLED, indicating the triplet utility *via* spin flipping. At the same time, this lifetime matches the high-lying reverse intersystem crossing (hRISC) time scale of HLCT.[54] Magneto-electroluminescence (MEL) measurements were performed to further validate the existence of hRISC in the

Table 2 EL performance of OLED[a]

Device	V_{on} (V)	L_{max} (cd m^{-2})	η_C (cd A^{-1})	η_P (lm W^{-1})	η_{ext} (%)	λ_{EL} (nm)	CIE (x, y)	FWHM (nm)	Blue index (cd A^{-1})
D1	3.8	1051	2.0	1.7	5.7	424	(0.167, 0.045)	27	44
S1	3.6	1242	1.7	1.4	6.1	424	(0.165, 0.036)	24	47
D2	3.6	3866	19.4	16.9	19.5	468	(0.133, 0.126)	29	154
S2	3.4	7679	25.0	23.1	25.0	468	(0.137, 0.123)	29	203

[a] The maximum luminance (L_{max}), current efficiency (η_c), power efficiency (η_P) and external quantum efficiency (η_{ext}) of the devices: maximum values. V_{on} = turn-on voltage at 1 cd m^{-2}. CIE coordinates at 4 V.

EL process. For the 4CzpICz-based device, the high-quality MEL traces were obtained to show saturation values at the higher magnetic field, excluding the occurrence of TTA process (Fig. S12).[55,56]

Using exciplex hosts confining high energy triplet excitons in the sensitizing system is an effective approach to optimize the EL efficiencies of the deep blue emitters, so the sensitized hyperfluorescence devices using triplet exciton harvesting host materials comprises a mixture of mCP and TSPO1 are constructed. S1 and S2 show slightly decreased driving voltages without shift of emission maxima, due to the triplet exciton harvesting host materials are also used as the charge transport materials. The color purity of S1 exhibits significant increase with FWHM of 24 nm and CIE*y* of 0.036. With the improvement of carrier mobility and exciton utility, the efficiencies of S2 increase significantly with maximal luminance, current efficiency, power efficiency and external quantum yield of 7679 cd m^{-2}, 25.0 cd A^{-1}, 23.1 lm W^{-1}, and 25.0%, respectively, while keeping color purity well with narrowband characteristics. Besides, the blue index (a key property for blue OLED defined as the ratio of current efficiency over *y* value of the Commission Internationale d'Éclairage) of S2 also increases significantly from 154 to 203 cd per A CIEy^{-1}.

To evaluate the practical application potential of the emitters. The device lifetime was tested for 4CzpICz-based OLED (device configuration: ITO/MoO_3 (6 nm)/NPB (50 nm)/TcTa (5 nm)/mCBP (5 nm)/1 wt% 4CzpICz: mCBP (20 nm)/TSPO1 (5 nm)/TPBi (30 nm)/LiF (1 nm)/Al) at an initial luminance of 1000 cd m^{-2}. The device exhibits a T_{90} (time to 90% initial luminance) of 5.8 hours and the lifetime curve is included in Fig. 4e of the SI. This lifetime performance is comparable to or better than many reported narrowband blue HLCT OLEDs (typically LT_{50} < 20 h under the same initial luminance), confirming the structural stability of 4CzpICz and its compatibility with the device architecture.

3 Conclusions

This study presents a novel strategy for constructing narrowband blue-emitting MR-HLCT molecules by incorporating rigid donors into an MR core. Two designed molecules exhibit excellent thermal stability and photophysical properties, enabling the fabrication of efficient blue OLEDs with FWHM <30 nm. Increasing CT components in MR molecules effectively utilizes high-lying triplet excitons through the HLCT mechanism. The 4CzpICz-based device sets a record 19.5% EQE for narrowband blue HLCT systems, combining high fluorescence yield and exciton utilization efficiency. When sensitized by an exciplex co-host, the optimized device demonstrates outstanding performance: 7679 cd m^{-2} maximum luminance, 25.0% EQE, and blue-index of 203 cd A^{-2}. This work not only delivers high-performance devices but also establishes an effective molecular design paradigm for blue MR-HLCT emitters.

Author contributions

X. J. F., H. L. and Z. Z. conceived and supervised the project. H. L. and T. M. synthesized and characterized the emitters, Y. F. and Z. C. carried out the theoretical calculations. J. Q. J. Z., and Y. F. measured the photophysical properties and performed OLED fabrication. X. J. F. wrote the original manuscript. All authors interpreted the results and contributed to reviewing and editing the manuscript.

Conflicts of interest

The authors declare no conflict of interest.

Data availability

The data supporting this article have been included as part of the supplementary information (SI). Supplementary information is available. See DOI: https://doi.org/10.1039/d5sc06259d.

Acknowledgements

We acknowledge the National Natural Science Foundation of China (22571064, U23A20594 and 22375066), the Guangdong Basic and Applied Basic Research Foundation (2023B1515040003) and the Interdisciplinary Research Project of Hangzhou Normal University (2024JCXK01). H. L. and J. Q. contributed equally to this work.

References

1 C. Yin, Y. Xin, T. Huang, Q. Zhang, L. Duan and D. Zhang, *Nat. Commun.*, 2025, **16**, 30.
2 S. Xiao, X. Cao, G. Chen, X. Yin, Z. Chen, J. Miao and C. Yang, *Angew. Chem., Int. Ed.*, 2025, **64**, e202418348.
3 W. Liu, W. Deng, W. Wang, H. Wu, C. Gao, Y. Xie, J. Zhao, X. Dong, Z. Zhao, Z. Zheng, Y. Chi, L. Duan, X. Zhan, Y. Zou, H. Wu, J. Peng and Y. Cao, *Nat. Photonics*, 2025, **19**, 650.
4 L. Xing, J. Wang, W.-C. Chen, B. Liu, G. Chen, X. Wang, J.-H. Tan, S. S. Chen, J.-X. Chen, S. Ji, Z. Zhao, M.-C. Tang and Y. Huo, *Nat. Commun.*, 2024, **15**, 6175.
5 X. Liu, L. Hua, X. Lai, J. H. Kim, Q. Zhu, J. Y. Lee, W. Zhu and Y. Wang, *Adv. Mater.*, 2025, **37**, 2500690.
6 J. M. Dos Santos, D. Hall, B. Basumatary, M. Bryden, D. Chen, P. Choudhary, T. Comerford, E. Crovini, A. Danos, J. De, S. Diesing, M. Fatahi, M. Griffin, A. K. Gupta, H. Hafeez, L. Hämmerling, E. Hanover, J. Haug, T. Heil, D. Karthik, S. Kumar, O. Lee, H. Li, F. Lucas, C. F. Ross Mackenzie, A. Mariko, T. Matulaitis, F. Millward, Y. Olivier, Q. Qi, I. D. W. Samuel, N. Sharma, C. Si, L. Spierling, P. Sudhakar, D. Sun, E. Tankelevičiūtė, M. D. Tonet, J. Wang, T. Wang, S. Wu, Y. Xu, L. Zhang and E. Zysman-Colman, *Chem. Rev.*, 2024, **124**, 13736.
7 U. Deori, G. P. Nanda, C. Murawski and P. Rajamalli, *Chem. Sci.*, 2024, **15**, 17739.

8 A. Nowak-Krol, P. T. Geppert and K. R. Naveen, *Chem. Sci.*, 2024, (15), 7408.
9 A. Farokhi, S. Lipinski, L. M. Cavinato, H. Shahroosvand, B. Pashaei, S. Karimi, S. Bellani, F. Bonaccorso and R. D. Costa, *Chem. Soc. Rev.*, 2025, **54**, 266.
10 C. Liao, S. Wang, B. Chen, Q. Xie, J. Feng, J. Bai, X. Li and H. Liu, *Angew. Chem., Int. Ed.*, 2025, **64**, e202414905.
11 S. K. Jeon, H. L. Lee, K. S. Yook and J. Y. Lee, *Adv. Mater.*, 2019, **31**, 1803524.
12 Y. Xu, Q. Wang, X. Cai, C. Li, S. Jiang and Y. Wang, *Angew. Chem., Int. Ed.*, 2023, **62**, e202312451.
13 W. Yuan, T. Huang, J. Zhou, M.-C. Tang, D. Zhang and L. Duan, *Nat. Commun.*, 2025, **16**, 4446.
14 J. Zhu, M. Huang, Y. Zhang, Z. Chen, Y. Deng, H. Zhang, X. Wang and C. Yang, *Angew. Chem., Int. Ed.*, 2025, **64**, e202418770.
15 M. A. Baldo, D. F. O'Brien, Y. You, A. Shoustikov, S. Sibley, M. E. Thompson and S. R. Forrest, *Nature*, 1998, **395**, 151.
16 C. Adachi, M. A. Baldo, M. E. Thompson and S. R. Forrest, *J. Appl. Phys.*, 2001, **90**, 5048.
17 Y. Ma, H. Zhang, J. Shen and C. Che, *Synth. Met.*, 1998, **94**, 245.
18 P. Ma, Y. Chen, Y. Man, Q. Qi, Y. Guo, H. Wang, Z. Li, P. Chang, C. Qu, C. Han and H. Xu, *Angew. Chem., Int. Ed.*, 2024, **63**, e202316479.
19 C. Zhang, W. Su, J. Sun, Y. Man, Y. Wei, C. Duan, C. Han and H. Xu, *Adv. Mater.*, 2025, **37**, 2502747.
20 J. Wang, P. Zou, L. Chen, Z. Bai, H. Liu, W.-C. Chen, Y. Huo, B. Z. Tang and Z. Zhao, *Light: Sci. Appl.*, 2024, **13**, 139.
21 Y. Fu, H. Liu, B. Z. Tang and Z. Zhao, *Nat. Commun.*, 2023, **14**, 2019.
22 A. Endo, M. Ogasawara, A. Takahashi, D. Yokoyama, Y. Kato and C. Adachi, *Adv. Mater.*, 2009, **21**, 4802.
23 G. Hong, X. Gan, C. Leonhardt, Z. Zhang, J. Seibert, J. M. Busch and S. Bräse, *Adv. Mater.*, 2021, **33**, 2005630.
24 X. Mu, T. Wang, D. Li, D. Liu, J. Wang, J. Li, S. Su, W. Li and Z. Ge, *Chin. Chem. Lett.*, 2025, 111986.
25 H. Zhang, G. Li, X. Guo, K. Zhang, B. Zhang, X. Guo, Y. Li, J. Fan, Z. Wang, D. Ma and B. Z. Tang, *Angew. Chem., Int. Ed.*, 2021, **60**, 22241.
26 F. Zhan, K. Xu, T. Tsuboi, Y. She and G. Li, *Angew. Chem., Int. Ed.*, 2025, **64**, e202505328.
27 T. Huang, Y. Xu, X. Lu, Y. Qu, J. Wei and Y. Wang, *Angew. Chem., Int. Ed.*, 2024, **63**, e202411268.
28 W. Li, D. Liu, F. Shen, D. Ma, Z. Wang, T. Feng, Y. Xu, B. Yang and Y. Ma, *Adv. Funct. Mater.*, 2012, **22**, 2797.
29 H. Hirai, K. Nakajima, S. Nakatsuka, K. Shiren, J. Ni, S. Nomura, T. Ikuta and T. Hatakeyama, *Angew. Chem., Int. Ed.*, 2015, **54**, 13581.
30 T. Hatakeyama, K. Shiren, K. Nakajima, S. Nomura, S. Nakatsuka, K. Kinoshita, J. Ni, Y. Ono and T. Ikuta, *Adv. Mater.*, 2016, **28**, 2777.
31 X. Xiong, T.-F. Chen, R. Walia, X.-. Fan, Y.-C. Cheng, H. Wang, H. Wu, X.-K. Chen, J. Yu, K. Wang and X.-H. Zhang, *Angew. Chem., Int. Ed.*, 2025, **64**, e202414882.
32 L. Wu, Z. Xin, D. Liu, D. Li, J. Zhang, Y. Zhou, S. Wu, T. Wang, S.-J. Su, W. Li and Z. Ge, *Adv. Mater.*, 2025, **37**, e2416224.
33 R.-H. Liu, Z.-Q. Feng, S.-J. Ge, Y. Wang, Z.-H. Yu, J.-R. Wu, H.-Y. Yan, D.-Y. Zhou, L.-S. Liao and Z.-Q. Jiang, *Angew. Chem., Int. Ed.*, 2025, **64**, e202424950.
34 X. Zeng, X. Luo, G. Meng, X. Wang, D. Zhang and L. Duan, *Angew. Chem., Int. Ed.*, 2025, **64**, e202423670.
35 X. Wu, S. Ni, C.-H. Wang, W. Zhu and P.-T. Chou, *Chem. Rev.*, 2025, **125**, 6685.
36 M. Mamada, M. Hayakawa, J. Ochi and T. Hatakeyama, *Chem. Soc. Rev.*, 2024, **53**, 1624.
37 X. Dong, J. Zeng, R. Sun, L. Xu, Z. Zhuang, J. Ye, B. Z. Tang and Z. Zhao, *ACS Mater. Lett.*, 2025, **7**, 457.
38 V. V. Patil, H. L. Lee, I. Kim, K. H. Lee, W. J. Chung, J. Kim, S. Park, H. Choi, W.-J. Son, S. Ok. Jeon and J. Y. Lee, *Adv. Sci.*, 2021, **8**, 2101137.
39 J. Kang, S. O. Jeon, H. L. Lee, J. Lim, U. Jo and J. Y. Lee, *Mater. Today*, 2023, **69**, 88.
40 T. Hua, X. Cao, J. Miao, X. Yin, Z. Chen, Z. Huang and C. Yang, *Nat. Photonics*, 2024, **18**, 1161.
41 S. M. Suresh, L. Zhang, T. Matulaitis, D. Hall, C. Si, G. Ricci, A. M. Z. Slawin, S. Warriner, D. Beljonne, Y. Olivier, I. D. W. Samuel and E. Zysman-Colman, *Adv. Mater.*, 2023, **35**, 2300997.
42 J. Jin, M. Chen, H. Jiang, B. Zhang, Z. Xie and W.-Y. Wong, *ACS Mater. Lett.*, 2024, **6**, 3246.
43 J. Wei, C. Zhang, D. Zhang, Y. Zhang, Z. Liu, Z. Li, G. Yu and L. Duan, *Angew. Chem., Int. Ed.*, 2021, **60**, 12269.
44 J. Ochi, Y. Yamasaki, K. Tanaka, Y. Kondo, K. Isayama, S. Oda, M. Kondo and T. Hatakeyama, *Nat. Commun.*, 2024, **15**, 2361.
45 H. L. Lee, J. Kang, J. Lim, S. C. Kim, S. O. Jeon and J. Y. Lee, *Nat. Commun.*, 2023, **14**, 4818.
46 Q. Peng, W. Yang, N. Li, S. Gong, X. Gao, C. Ye, Y. Zou and C. Yang, *Chem. Eng. J.*, 2023, **466**, 143423.
47 H. L. Lee, W. J. Chung and J. Y. Lee, *Small*, 2020, **16**, 1907569.
48 R. Gao, X. Li, X. Tian, R. Yang, Y. Luo, Z. Jia, J. Huang, H. Xu, Y. Miao, H. Wang, J. Li and Z. Zhao, *Chem. Eng. J.*, 2025, **524**, 169570.
49 X.-Q. Gan, Z.-M. Ding, D.-H. Liu, W.-Q. Zheng, B. Ma, H. Zhang, X. Chang, L. Wang, Y. Liu, X. Wu, S.-J. Su and W. Zhu, *Adv. Opt. Mater.*, 2023, **11**, 2300195.
50 X. He, J. Lou, B. Li, X. Dong, F. Zhong, W. Liu, X. Feng, D. Yang, D. Ma, Z. Zhao, Z. Wang and B. Z. Tang, *Adv. Mater.*, 2024, **36**, 2310417.
51 K. Jiang, X. Chang, J. Zhu, T. Zhu, J. Yu, Y. Wang, Y. Zhang, D. Ma and W. Zhu, *Angew. Chem., Int. Ed.*, 2025, **64**, e202421520.
52 J. Liu, Y. Zhu, T. Tsuboi, C. Deng, W. Lou, D. Wang, T. Liu and Q. Zhang, *Nat. Commun.*, 2022, **13**, 4876.
53 Z. Zhong, X. Zhu, X. Wang, Y. Zheng, S. Geng, Z. Zhou, X. J. Feng, Z. Zhao and H. Lu, *Adv. Funct. Mater.*, 2022, **32**, 2112969.
54 K. Zhang, Z. Zhou, D. Liu, Y. Chen, S. Zhang, J. Pan, X. Qiao, D. Ma, S. Su, W. Zhu and Y. Liu, *Angew. Chem., Int. Ed.*, 2024, **63**, e202407502.

55 X. Guo, P. Yuan, J. Fan, X. Qiao, D. Yang, Y. Dai, Q. Sun, A. Qin, B. Z. Tang and D. Ma, *Adv. Mater.*, 2021, **33**, 2006953.

56 Y. Xu, X. Liang, X. Zhou, P. Yuan, J. Zhou, C. Wang, B. Li, D. Hu, X. Qiao, X. Jiang, L. Liu, S.-J. Su, D. Ma and Y. Ma, *Adv. Mater.*, 2019, **31**, 1807388.